Impact of TP53-induced glycolysis and apoptosis regulator on malignant activity and resistance to ferroptosis in intrahepatic cholangiocarcinoma

利田, 賢哉

Received: 13 July 2023 | Revised: 12 September 2023 | Accepted: 15 September 2023

DOI: 10.1111/cas.15981

Cancer Science WILEY

ORIGINAL ARTICLE

Impact of *TP53*-induced glycolysis and apoptosis regulator on malignant activity and resistance to ferroptosis in intrahepatic cholangiocarcinoma

Katsuya Toshida[1] | Shinji Itoh[1] | Norifumi Iseda[1] | Takuma Izumi[1] | Shohei Yoshiya[1] | Takeo Toshima[1] | Mizuki Ninomiya[1] | Takeshi Iwasaki[2] | Yoshinao Oda[2] | Tomoharu Yoshizumi[1]

[1]Department of Surgery and Science, Graduate School of Medical Sciences, Kyushu University, Fukuoka, Japan

[2]Department of Anatomic Pathology, Graduate School of Medical Sciences, Kyushu University, Fukuoka, Japan

Correspondence
Shinji Itoh, Department of Surgery and Science, Graduate School of Medical Sciences Kyushu University, 3-1-1, Maidashi, Fukuoka 812-8582, Japan.
Email: itoh.shinji.453@m.kyushu-u.ac.jp

Funding information
Japan Society for the Promotion of Science, Grant/Award Number: JP-19K09198 and JP-23K08133; the Kobayashi Foundation for Cancer Research; the Takeda Science Foundation

Abstract

TP53-induced glycolysis and apoptosis regulator (*TIGAR*) is an important gene that encodes a regulatory enzyme of glycolysis and reactive oxygen species (ROS) detoxification and is associated with worse prognosis in various cancers. Ferroptosis is a recently identified type of programmed cell death that is triggered by iron-dependent lipid peroxidation. There are no reports on the prognostic impact of TIGAR on intrahepatic cholangiocarcinoma (ICC), and its role in ferroptosis is unclear. Ninety ICC patients who had undergone hepatic resection were enrolled. Immunohistochemical staining for TIGAR was performed. The regulation of malignant activity by TIGAR and the association between ferroptosis and TIGAR were investigated in vitro. Twenty-two (24.4%) patients were categorized into TIGAR-high and -low groups by immunohistochemical staining. There were no noticeable differences in background factors between the two groups, but TIGAR positivity was an independent prognostic factor in disease-free survival (hazard ratio [HR], 2.00; 95% confidence interval [CI], 1.04–3.85, $p=0.0378$) and overall survival (HR, 2.10; 95% CI, 1.03–4.30, $p=0.00422$) in a multivariate analysis. In vitro, *TIGAR* knockdown (KD) decreased cell motility (cell proliferation/migration/invasion/colony-forming capabilities) and elevated ROS and lipid peroxidation. This indicated that *TIGAR* KD induced ferroptosis. *TIGAR* KD-induced ferroptosis was suppressed using liproxstatin. *TIGAR* KD decreased the expression of glutathione peroxidase 4, known as factor-suppressing ferroptosis. The combination of *TIGAR* KD with cisplatin significantly induced more ferroptosis. In conclusion, TIGAR is associated with poor outcomes in ICC patients and resistance to ferroptosis.

Abbreviations: ALP, alkaline phosphatase; CA19-9, carbohydrate antigen 19-9; CDDP, cisplatin; CEA, carcinoembryonic antigen; CI, confidence interval; DFS, disease-free survival; GEO, gene expression omnibus; G6PD, glucose-6-phosphonate dehydrogenase; GSGG, oxidized glutathione; GSH, reduced glutathione; GPX4, glutathione peroxidase 4; HR, hazard ratio; HBV-Ag, hepatitis B surface-antigen; HCV-Ab, hepatitis C virus-antibody; ICC, intrahepatic cholangiocarcinoma; MDA, malondialdehyde; NADP, nicotinamide adenine dinucleotide phosphate; NADPH, nicotinamide adenine dinucleotide phosphate; Nrf2, nuclear factor erythroid 2-related factor 2; OS, overall survival; RNA, ribonucleic acid; ROS, reactive oxygen species; TIGAR, *TP53*-induced glycolysis and apoptosis regulator; xCT, system Xc^-; γ-GTP, γ-glutamyl transpeptidase.

KEYWORDS
cisplatin, ferroptosis, intrahepatic cholangiocarcinoma, *TP53*-induced glycolysis and apoptosis regulator

1 | INTRODUCTION

Intrahepatic cholangiocarcinoma (ICC) is the second most common primary liver malignancy after hepatocellular carcinoma, comprising approximmately 15%, and its incidence has increased worldwide in the past few decades.[1] The only potentially curative treatment for ICC is hepatic resection, but its recurrence rate remains high.[2,3] Systemic therapy with gemcitabine plus cisplatin (CDDP) has been performed for locally advanced, metastatic, and recurrent ICC.[4] Recently, research on drug resistance and fusion genes, such as fibroblast growth factor receptor 2, has been conducted.[5,6]

TP53-induced glycolysis and apoptosis regulator (*TIGAR*) was identified as an important gene that encodes a regulatory enzyme of glycolysis and reactive oxygen species (ROS) detoxification.[7] TIGAR contributes to the production of nicotinamide adenine dinucleotide phosphate (NADPH) by promoting the pentose phosphate pathway. Because of its role, it has been reported that dynamic ROS control by TIGAR regulates cancer initiation and progression in pancreatic cancer.[8] In other carcinomas, such as breast and colorectal cancer, high TIGAR expression is reported to be associated with a worse prognosis.[9,10]

In cancer research, it is important to efficiently kill cancer cells while leaving healthy cells intact. Cancer cells often have defective cell death execution mechanisms, which is one of the main reasons for their resistance to therapy. Ferroptosis was first proposed by Dixon et al. in 2012 as an iron-dependent regulated cell death mechanism, occurring through excessive peroxidation of polyunsaturated fatty acids.[11] While ferroptosis plays an important role in cell metabolism, resistance to ferroptosis in cancer cells has recently attracted attention, and establishing how to induce ferroptosis in cancer cells is important in cancer therapy.[12] However, the potential importance of ferroptosis in cancer therapy is not yet fully understood.

To our best knowledge, there is no report showing the impact of TIGAR on the prognosis of ICC patients, and its association with ferroptosis remains unclear. This study aimed to demonstrate the prognostic impact of TIGAR and its critical role in resistance to ferroptosis in ICC.

2 | MATERIALS AND METHODS

2.1 | Patients and specimen preparation

This retrospective study was approved by the ethics committee of Kyushu University Hospital. We retrospectively enrolled 90 patients who had undergone hepatic resection for primary ICC without preoperative chemotherapy or radiation. This study was conducted by reviewing the patients' medical records from May 1993 to December 2020 at Kyushu University Hospital in Japan. The detailed surgical procedure for hepatic resection has previously been described.[13] The specimens were fixed in 10% formalin solution, embedded in paraffin, and sectioned into 4-μm-thick slices to evaluate the histological features.

2.2 | Data collection of clinicopathological characteristics

Patient data were recorded, including age, sex, hepatitis B surface antigen (HBV-Ag) positivity, hepatitis C virus-antibody (HCV-Ab) positivity, total bilirubin, alkaline phosphatase, γ-glutamyl transpeptidase, albumin, platelet count, carcinoembryonic antigen, carbohydrate antigen 19-9 (CA19-9), maximum tumor size, tumor localization, poor differentiation, microvascular invasion, intrahepatic metastasis, lymph node metastasis, and histological liver cirrhosis.

2.3 | Follow-up strategy

All patients underwent monthly screening for recurrence by undergoing computed tomography every 3 months and testing for tumor markers every month after discharge. If recurrence was suspected, MRI was conducted and we diagnosed the presence or absence of recurrence. Overall survival (OS) was defined as the time from treatment to death, regardless of disease recurrence. Disease-free survival (DFS) was defined as the time from hepatic resection to tumor recurrence or death.

2.4 | Data acquisition and preprocessing

We downloaded three sets of ribonucleic acid (RNA) expression data with patient prognostic information from the GSE107943 dataset of the Gene Expression Omnibus (GEO) database (https://www.ncbi.nlm.nih.gov/geo/). iDEP is an integrated web application that incorporates differential expression and pathway analyses to help biologists interpret read counts or other types of expression matrices derived from read mapping. We performed transcriptomic analyses of GSE107943 by iDEP.

2.5 | Immunohistochemistry

Immunohistochemical staining was performed as previously described.[14] Formalin-fixed, paraffin-embedded tissue sections from

patients with ICC were immunostained for anti-rabbit TIGAR antibody (1:500 dilution; Abcam) and anti-mouse 4-hydroxy-2-nonenal (4-HNE) antibody (1:50 dilution; Japan Institute for the Control of Aging) overnight at 4°C. After adding secondary antibodies and incubating at room temperature for 1 h, color development was performed using 3,3-diamino-benzidine, followed by counterstaining with Mayer's hematoxylin. Stained slides were scanned by NanoZoomer (Hamamatsu Photonics KK) and three experienced researchers (K.T., S.I., and T.I.) who were blinded to the patient's clinical status when evaluating immunohistochemical data. The evaluation method and cut-off value of TIGAR were previously reported, and staining cell intensity was graded as follows: 0 = negative; 1 = weakly positive; 2 = moderately positive; and 3 = positive. The proportion of tumor cells was defined as follows: 0 = less than 5%; 1 = 5%–25%; 2 = 26%–50%; 3 = 51%–75%; and 4 = greater than 75%. The score was determined by the product of cell staining intensity and the proportion of tumor cells. Staining intensity 0–7 was defined as low expression while staining intensity 8–12 was defined as high expression.[15] The evaluation method of 4-HNE was previously reported, and staining cell intensity was graded as follows: 0 = negative; 1 = weakly positive; 2 = moderately positive; and 3 = positive. The percentage of stained cells ranged from 0 to 100%. Then, we multiplied the intensity and percentage scores to obtain the final expression score.[16]

2.6 | Cell culture and reagents

Two ICC cell lines, HuCCT1 and SSP-25 (Riken Cell Bank), were cultured in RPMI medium (Thermo Fisher Scientific) supplemented with 10% FBS in a humidified atmosphere of 5% CO_2 at 37°C. Negative control and *TIGAR* siRNA (TriFECTa Kit DsiRNA Duplex) were purchased from Integrated DNA Technology and transfected 48 h after seeding cells by forward transfection using Lipofectamine RNAiMAX (Thermo Fisher Scientific) according to the manufacturer's instructions. Cellular ROS assay kit, glycolysis assay, NADP/NADPH assay, and oxidized glutathione (GSSG)/reduced glutathione (GSH) quantification kits were purchased from Dojindo (cat. 340-09811, 343-09921, 344-09331, and 342-09011, respectively; Kumamoto, Japan). A malondialdehyde (MDA) assay kit was purchased from JaICA (cat. KMD-008W). A liproxstatin and caspase-3/7 fluorescence assay kit was purchased from Cayman-Chemical (cat. 950455-15-9 and cat. 10009135). CDDP was purchased from Sigma-Aldrich (cat. 15663-27-1).

2.7 | Real-time polymerase chain reaction

RNA extraction was performed using the Maxwell RSC RNA cells and RNA tissue kit (Promega). Complementary DNA was synthesized using a SuperScript cDNA synthesis kit (Invitrogen). We performed RT-PCR with a StepOnePlus System (Applied Biosystems) using SYBR Green PCR Master Mix (Applied Biosystems). Relative gene expression was normalized to β-actin mRNA and calculated using the delta–delta CT method. The human glucose-6-phosphonate dehydrogenase (G6PD) RT-PCR forward and reverse primers were 5′-CTGTTCCGTGAGGACCAGATCT-3′ and 5′-TGAAGGTGAGGATA ACGCAGGC-3′, respectively.

2.8 | Western blotting analysis

After collecting the cells and extracting the proteins, samples were heated at 95°C for 5 min and subjected to electrophoresis using SuperSep Ace 10% gels (Fujifilm) at 20 mA for 80 min. The proteins were transferred onto a polyvinylidene difluoride membrane using the Trans-Blot Turbo Transfer System (Bio-Rad). Primary and secondary antibodies were diluted in iBind solution (Invitrogen); the primary antibodies were anti-rabbit TIGAR (1:1000; Proteintech), anti-rabbit glutathione peroxidase 4 (GPX4; 1:1000 dilution; Abcam), anti-rabbit nuclear factor erythroid 2-related factor 2 (Nrf2) antibody (1:1000 dilution; Abcam), and anti-rabbit β-actin (1:5000; GeneTex), and the secondary antibody was goat anti-rabbit IgG H&L (1:5000; Abcam). The membrane was incubated in iBind solution with both primary and secondary antibodies. Each blot was incubated with Chemiluminescent HRP Antibody Detection Reagent (Denville Scientific) and imaged using an Amersham Imager 600 (GE Healthcare).

2.9 | Assessment of cell viability

Cell viability was evaluated using a Celltiter-Glo luminescent cell viability assay kit (cat. G7570; Promega), which determined cellular viability by measuring ATP levels 48 h after cell seeding.

2.10 | Assessment of invasion, migration, and colony formation abilities

For invasion assays, a Falcon Permeable Support was added to a six-well plate with 15 μL 5 mg/mL Matrigel Matrix (Corning) on an 8-μm Transparent PET Membrane (Corning) 48 h after seeding. The infiltrated cells were stained with Diff-Quik (JACLaS) on the Transwell membrane surface, counted in five randomly selected fields at ×200 magnification, and quantified using Image J software (https://imagej.net/). Cells were seeded in a six-well flat-bottomed plate and incubated until 90% confluency. Confluent cell monolayers were scratched using plastic tips. Images of scratched areas were captured 24 h after scratching and evaluated as the percentage of migration (migration index: 1–[length at 24 h]/[length at 0 h]). Cells were seeded in six-well flat-bottomed plates in RPMI supplemented with 10% FBS. After 10 days of culture, colonies were fixed and stained with Diff-Quik. The number of colonies was counted using Image J software (https://imagej.net/).

2.11 | Evaluation of intracellular reactive oxygen species and lipid peroxidation

We measured intracellular ROS and MDA as previously described.[17,18] Cells were seeded in 500 μL 10% FBS RPMI medium in 24-well clear bottomed plates (20,000 cells/well) and incubated at 37°C for 48 h in 10% CO_2. After washing cells with HBSS, cells were incubated with 10 mM DCFH-DA at 37°C for 30 min. Subsequently, we performed fluorescent microplate measurements and measured the fluorescence of cells to assess the amount of intracellular ROS. Next, we evaluated lipid peroxidation using an MDA assay kit. Cells were seeded into 24-well plates (20,000 cells/well) and incubated at 37°C for 48 h in 10% CO_2. After the addition of butylated hydroxytoluene, 2-thiobarbituric acid, and acid reagent were added to samples, which were incubated at 60°C for 60 min. Subsequently, we collected the supernatant after centrifugation at 10,000 *g* for several minutes and subjected it to optical density measurement at 532 nm on a microplate reader. ROS and MDA levels were normalized by cell viability to calculate ROS/cell viability and MDA/cell viability.[19]

2.12 | Glycolysis assay

Glycolysis analysis was performed using a Glycolysis Assay Kit. Cells (20,000/well) after *TIGAR* knockdown (KD) were seeded into a 24-well plate. The glycolytic activity was evaluated by inhibiting adenosine triphosphate synthesis by oxidative phosphorylation with oligomycin and measuring the change in lactate content (absorbance).

2.13 | GSH/GSGG assay

GSH/GSGG analysis was performed using a GSSG/GSH Quantification Kit. Cells (20,000/well) after *TIGAR* KD were seeded into a 24-well plate. Cells were homogenized with 500 μL methanol, homogenates were centrifuged at 12,000 *g* at 4°C for 5 min, and supernatants were collected. Cell homogenates were dried at room temperature under reduced pressure, and the residue was dissolved in 100 μL purified water containing 1.97 μM 5-sulfosalicylic acid. GSSG/GSH quantification was determined based on fluorescence intensity in cells using a microplate reader.

2.14 | NADP/NADPH assay

Cells (50,000/well) after *TIGAR* KD were seeded into a 24-well plate and incubated at 37°C for 48 h in 10% CO_2. The intracellular levels of reductive NADP+/NADPH were determined based on the fluorescence intensity in cells using a microplate reader (BioTek) according to the manufacturer's instructions.

2.15 | Caspase-3/7 fluorescence assay

Cells (50,000/well) after *TIGAR* KD were seeded into a 96-well plate and incubated at 37°C for 48 h in 10% CO_2. Caspase-3/-7 analysis was performed using a caspase-3/-7 fluorescence assay kit; caspase-3/-7 activity was determined based on the fluorescence intensity in cells using a microplate reader, according to the manufacturer's instructions.

2.16 | Statistical analysis

All statistical analyses were performed using SAS software (JMP Pro 15; SAS Institute). The Shapiro–Wilk test was used to assess whether continuous variables were normally distributed. Continuous variables were presented as the median and were compared using the Mann–Whitney *U*-test. Categorical variables were reported as percentages and compared using the χ^2-test or Fisher's exact test. Cumulative DFS and OS rates were calculated using the Kaplan–Meier method, and differences between the curves were evaluated using the log-rank test. Survival data were used to establish a univariate Cox proportional hazards model. Covariates that were significant at $p < 0.05$ were included in the multivariate Cox proportional hazards model.

3 | RESULTS

3.1 | Association between *TP53*-induced glycolysis and apoptosis regulator expression and clinicopathological characteristics

In our study of 90 patients with ICC, 58 patients were male (64.4%). The median age of the patients was 66 years (range, 33–87 years). Figure 1A shows representative immunohistochemical staining for TIGAR in ICC tissues, and TIGAR expression was observed in the cytoplasm. Twenty-two patients (24.4%) were high for TIGAR by immunohistochemistry. The associations between TIGAR expression and patient clinicopathological factors are shown in Table 1. The TIGAR-high group contained less HBs-Ag positivity ($p = 0.0143$) and more HCV-Ab positivity ($p = 0.0087$), but there was no significant difference in pathological factors.

3.2 | Univariate survival analysis of patients with intrahepatic cholangiocarcinoma according to *TP53*-induced glycolysis and apoptosis regulator expression

We assessed the association between TIGAR expression and patient postoperative survival after hepatic resection using the Kaplan–Meier method (Figure 1B,C). The median DFS was 3.19 years (range, 1.17–9.86 years) in the TIGAR-negative group and 1.16 years (range,

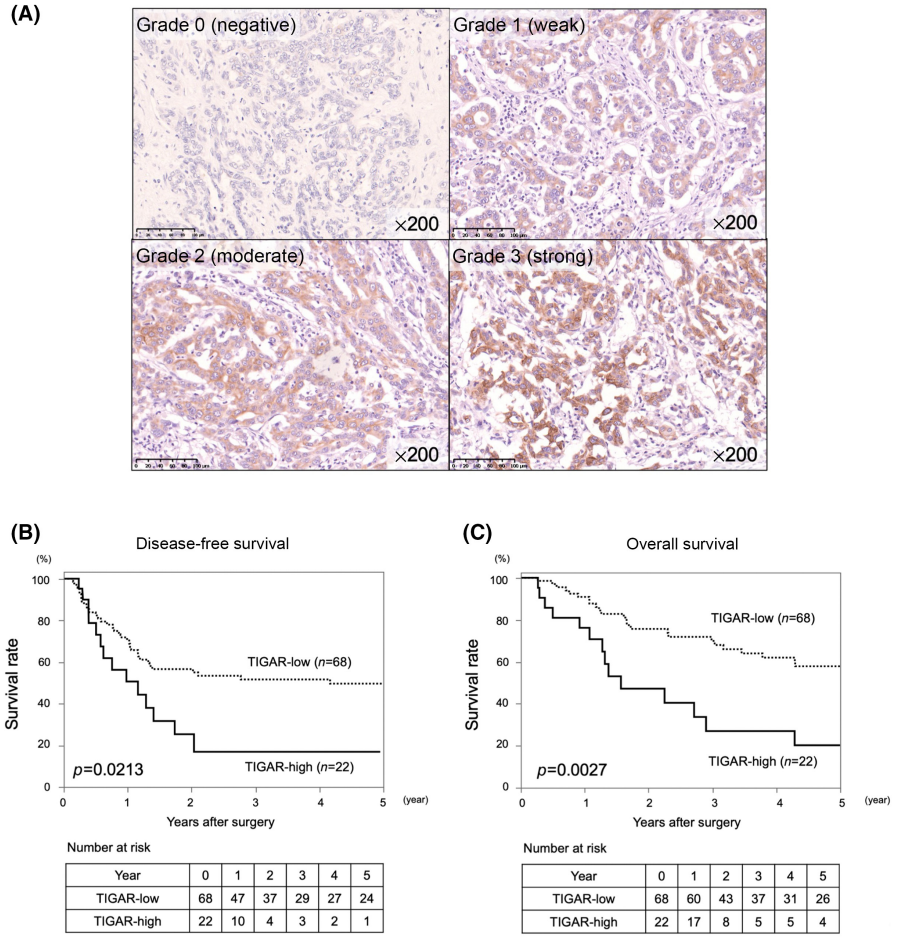

FIGURE 1 *TP53*-induced glycolysis and apoptosis regulator (TIGAR) is an indicator of poor prognosis in our cohort. (A) Immunohistochemical staining of TIGAR. Grade 0, negative staining; Grade 1, weak staining; Grade 2, moderate staining; Grade 3, strong staining (×200 magnification). (B) Disease-free survival (DFS) and (C) overall survival (OS) in intrahepatic cholangiocarcinoma (ICC) patients according to TIGAR expression in our cohort. TIGAR, *TP53*-induced glycolysis and apoptosis regulator.

0.51–1.74) in the TIGAR-high group. Median OS was 8.15 years (range, 3.78–NA years) in the TIGAR-negative group and 2.25 years (range, 1.28–4.29 years) in the TIGAR-high group. Kaplan–Meier also analysis revealed the trend towards significantly impaired DFS ($p=0.0213$) and OS ($p=0.0027$) in the TIGAR-high group.

3.3 | Risk factors associated with disease-free survival

Table 2 lists the univariate and multivariate analyses results associated with DFS in patients with ICC after hepatic resection. Univariate analysis of the association between DFS and patient characteristics showed that the significant prognostic factors were maximum tumor size (≥5 cm; hazard ratio [HR], 2.50; 95% confidence interval [CI], 1.44–4.35; $p=0.0011$), tumor localization (perihilar type; HR, 2.04; 95% CI, 1.15–3.59; $p=0.0142$), intrahepatic metastasis (HR, 2.96; 95% CI, 1.71–5.15; $p=0.0001$), microvascular invasion (HR, 3.51; 95% CI, 1.91–6.44; $p<0.0001$), lymph node metastasis (HR, 3.15; 95% CI, 1.72–5.77; $p=0.0002$), and TIGAR positivity (HR, 2.07; 95% CI, 1.10–3.91; $p=0.0243$). Multivariate analysis also showed that the independent prognostic factors for DFS were maximum tumor size (≥5 cm) (HR, 2.75; 95% CI, 1.52–4.99; $p=0.0008$), tumor localization (perihilar type; HR, 2.50; 95% CI, 1.25–5.01; $p=0.0098$), microvascular invasion (HR, 2.31; 95% CI, 1.13–4.73; $p=0.0214$), and TIGAR positivity (HR, 2.00; 95% CI, 1.04–3.85; $p=0.0378$).

3.4 | Risk factors associated with overall survival

Table 3 lists the univariate and multivariate analyses results associated with OS in patients with ICC after hepatic resection. Univariate analysis of the association between OS and patient characteristics showed that the significant prognostic factors were albumin (≤4.0 g/dL; HR, 1.81; 95%CI, 1.00–3.28; $p=0.0488$), CA19-9 (≥38 U/mL; HR, 2.18; 95% CI, 1.18–4.00; $p=0.0123$), maximum tumor size (≥5 cm; HR, 2.38; 95% CI, 1.31–4.33; $p=0.0042$), tumor localization (perihilar type; HR, 2.60; 95% CI, 1.36–4.97; $p=0.0038$), intrahepatic metastasis (HR, 2.61; 95% CI, 1.45–4.73; $p=0.0015$), microvascular invasion (HR, 2.40; 95% CI, 1.29–4.46; $p=0.0053$), lymph node metastasis (HR, 4.62; 95% CI, 2.44–8.74; $p<0.0001$), and TIGAR positivity (HR, 2.60; 95% CI, 1.36–4.97; $p=0.0038$). Multivariate analysis also showed that independent prognostic factors for DFS were albumin (≤4.0 g/dL; HR, 2.08; 95% CI, 1.09–3.97; $p=0.0263$), maximum tumor size (≥5 cm; HR, 2.82; 95% CI, 1.43–5.56; $p=0.0027$), tumor localization (perihilar type; HR, 2.12; 95% CI, 1.04–4.33; $p=0.0389$), lymph node metastasis (HR, 2.81; 95% CI, 1.30–6.04; $p=0.0084$), and TIGAR positivity (HR, 2.10; 95% CI, 1.03–4.30; $p=0.0422$).

TABLE 1 Comparison of clinicopathological characteristics of patients with TIGAR-negative and positive following hepatic resection of ICC.

Factors	TIGAR-low ($n=68$)	TIGAR-high ($n=22$)	p-value
Age (years)	66 (33–87)	64 (41–80)	0.8877
Sex, male/female	42/26	16/6	0.3434
HBs-Ag positive	10 (14.1%)	0 (0%)	0.0143
HCV-Ab positive	2 (2.9%)	5 (22.7%)	0.0087
Total bilirubin (mg/dL)	0.7 (0.3–8.7)	0.7 (0.2–1.8)	0.9854
ALP (U/L)	304 (125–1337)	369 (174–1344)	0.6547
γ-GTP (IU/L)	75 (16–1071)	94 (21–472)	0.8604
Albumin (g/dL)	4.1 (3.2–5.3)	4.1 (2.9–4.9)	0.8130
Platelet count (10^4 μL)	20.0 (6.1–54.3)	20.1 (5.2–42.0)	0.8054
CEA (ng/mL)	2.4 (0.1–41.8)	2.8 (0.4–117)	0.1875
CA19-9 (U/mL)	37 (0.1–40,795)	36.0 (1.1–98,106)	0.2596
Maximum tumor size (cm)	4.1 (1.1–12.0)	4.0 (1.9–8.5)	0.6672
Tumor localization (peripheral type/perihilar type)	48/20	16/6	0.8468
Poor differentiation (%)	40 (58.8%)	14 (63.6%)	0.6876
Microvascular invasion (%)	32 (47.1%)	13 (59.1%)	0.3265
Intrahepatic metastasis (%)	22 (32.4%)	7 (31.8%)	0.9628
Lymph node metastasis (%)	13 (19.1%)	6 (27.3%)	0.4152
Histological liver cirrhosis (%)	6 (8.8%)	3 (13.6%)	0.6829

Note: Data are presented as *n* (%) or the median (range).

Abbreviations: ALP, alkaline phosphatase; CA19-9, carbohydrate antigen 19–9; CEA, carcinoembryonic antigen; HBs-Ag, hepatitis B surface antigen; HCV-Ab, hepatitis C virus antibody; ICC, intrahepatic cholangiocarcinoma; TIGAR, *TP53*-induced glycolysis and apoptosis regulator; γ-GTP, γ-glutamyl transpeptidase.

TABLE 2 Univariate and multivariate analyses of factors related to DFS in patients with ICC.

	Univariate analysis		Multivariate analysis	
Factors	HR (95% CI)	p-value	HR (95% CI)	p-value
Age (≥70 years)	1.10 (0.61–1.97)	0.7541		
Sex, male	1.22 (0.68–2.18)	0.4878		
Albumin (≤4.0 g/dL)	1.34 (0.77–2.33)	0.2879		
CA19-9 (≥38 U/mL)	1.64 (0.94–2.88)	0.0777		
Maximum tumor size (≥5 cm)	2.50 (1.44–4.35)	0.0011	2.75 (1.52–4.99)	0.0008
Tumor localization (perihilar type)	2.04 (1.15–3.59)	0.0142	2.50 (1.25–5.01)	0.0098
Poor differentiation	1.55 (0.88–2.75)	0.1271		
Intrahepatic metastasis	2.96 (1.71–5.15)	0.0001	1.63 (0.81–3.26)	0.1665
Micro vascular invasion	3.51 (1.91–6.44)	<0.0001	2.31 (1.13–4.73)	0.0214
Lymph node metastasis	3.15 (1.72–5.77)	0.0002	1.38 (0.63–2.99)	0.4122
TIGAR-high	2.07 (1.10–3.91)	0.0243	2.00 (1.04–3.85)	0.0378
Histological liver cirrhosis	1.02 (0.40–2.59)	0.9503		

Abbreviations: CA19-9, carbohydrate antigen 19-9; CI, confidence interval; DFS, disease-free survival; HR, hazard ratio; ICC, intrahepatic cholangiocarcinoma; TIGAR, *TP53*-induced glycolysis and apoptosis regulator.

3.5 | *TP53*-induced glycolysis and apoptosis regulator knockdown affects biological behaviors in intrahepatic cholangiocarcinoma cell lines

We confirmed the biological function of TIGAR using ICC cell lines HuCCT1 and SSP-25. Western blot assay verified a significant reduction in *TIGAR* expression upon siRNA treatment (Figure 2A). In addition, the results of viability, invasion, colony formation, and scratch assays indicated that *TIGAR* KD suppressed cell motility of ICC cells compared with the negative control (Figure 2B–E). In addition, we performed transcriptomic analysis to examine functional changes between the high- and low-*TIGAR* expression groups using a GEO dataset. When divided into TIGAR-high/-low groups according to *TIGAR* expression, the cases were clearly stratified (Figure S1A,B).

TABLE 3 Univariate and multivariate analyses of factors related to OS in patients with ICC.

	Univariate analysis		Multivariate analysis	
Factors	HR (95% CI)	*p*-value	HR (95% CI)	*p*-value
Age (≥70 years)	1.49 (0.80–2.77)	0.2023		
Sex, Male	1.24 (0.66–2.31)	0.4947		
Albumin (≤4.0 g/dL)	1.81 (1.00–3.28)	0.0488	2.08 (1.09–3.97)	0.0263
CA19-9 (≥38 U/mL)	2.18 (1.18–4.00)	0.0123	1.72 (0.90–3.29)	0.0999
Maximum tumor size (≥5 cm)	2.38 (1.31–4.33)	0.0042	2.82 (1.43–5.56)	0.0027
Tumor localization (perihilar type)	2.60 (1.36–4.97)	0.0038	2.12 (1.04–4.33)	0.0389
Poor differentiation	1.20 (0.67–2.18)	0.5364		
Intrahepatic metastasis	2.61 (1.45–4.73)	0.0015	1.53 (0.70–2.34)	0.3562
Microvascular invasion	2.40 (1.29–4.46)	0.0053	1.71 (0.79–3.71)	0.1772
Lymph node metastasis	4.62 (2.44–8.74)	<0.0001	2.81 (1.30–6.04)	0.0084
TIGAR-high	2.60 (1.36–4.97)	0.0038	2.10 (1.03–4.30)	0.0422
Histological liver cirrhosis	1.13 (0.40–3.17)	0.8190		

Abbreviations: CA19-9, carbohydrate antigen 19-9; CI, confidence interval; HR, hazard ratio; ICC, intrahepatic cholangiocarcinoma; OS, overall survival; TIGAR, *TP53*-induced glycolysis and apoptosis regulator.

Gene set enrichment analysis showed that lipid oxidation was upregulated in the *TIGAR*-low group.

3.6 | *TP53*-induced glycolysis and apoptosis regulator is associated with ferroptosis in intrahepatic cholangiocarcinoma cell lines

TIGAR regulates intracellular oxidative stress, and its association with ferroptosis was investigated. We examined the effect of *TIGAR* KD on ROS and lipid peroxidation. First, *TIGAR* KD significantly increased ROS levels (Figure 3A) and upregulated MDA levels (Figure 3B). Using liproxstatin, known as lipid peroxidation inhibitor, ferroptosis, ROS levels, and MDA levels were significantly inhibited by *TIGAR* KD (Figure 3C,D). Next, we investigated how *TIGAR* KD induces ferroptosis. TIGAR is known to increase NADPH production by promoting the pentose phosphate cycle and preventing glycolysis, and G6PD is the only rate-limiting enzyme in it; thus, we assessed the change in glycolysis, G6PD expression, and NADPH production by *TIGAR* KD. *TIGAR* KD significantly increased glycolysis level and decreased G6PD mRNA expression (Figure 3E,F). There was no significant difference in total NADP+ and NADPH, but the NADP+/NADPH ratio was significantly elevated by *TIGAR* KD (Figure 3G). Similarly, the GSGG/GSH ratio was also significantly increased (Figure 3H) and GPX4 protein levels were decreased by *TIGAR* KD (Figure 3I).

3.7 | Association between 4-HNE and *TP53*-induced glycolysis and apoptosis regulator

4-HNE protein has been described as a reliable and stable marker of lipid peroxidation in liver disease. We examined the association between 4-HNE and TIGAR expression in ICC tissue. Figure 4A shows representative immunohistochemical staining for 4-HNE in ICC tissues, and 4-HNE expression was observed in the cytoplasm. The median score of 4-HNE was 20, and the cut-off values for the score were determined by ROC curves (cut-off, 60; area under the curve, 0.58). The number of 4-HNE positive cases was 18 (26.5%) in the TIGAR-low group and 1 (4.6%) in the TIGAR-high group, with significantly fewer cases in the TIGAR-high group ($p=0.0345$; Figure 4B).

3.8 | *TP53*-induced glycolysis and apoptosis regulator induces not only ferroptosis but also apoptosis

As its name suggests, TIGAR is an apoptosis regulator and suppresses apoptosis; hence, we confirmed whether TIGAR is associated with apoptosis in ICC cell lines. *TIGAR* KD significantly elevated caspase 3/7 activity (Figure S2A) and the BAX/BCL-2 ratio (Figure S2B). These findings indicated that TIGAR regulated apoptosis in ICC.

3.9 | Induction of ferroptosis by *TP53*-induced glycolysis and apoptosis regulator knockdown in combination with CDDP

CDDP is a systemic therapy for ICC patients. We next examined the effect of *TIGAR* KD in combination with CDDP on cell viability, ROS, and lipid peroxidation. At first, we confirmed that the use of CDDP did not change the TIGAR protein expression (Figure S3). *TIGAR* KD and CDDP treatment significantly decreased cell viability (Figure 5A), increased ROS levels (Figure 5B), and increased MDA levels (Figure 5C) compared with *TIGAR* KD alone and CDDP alone.

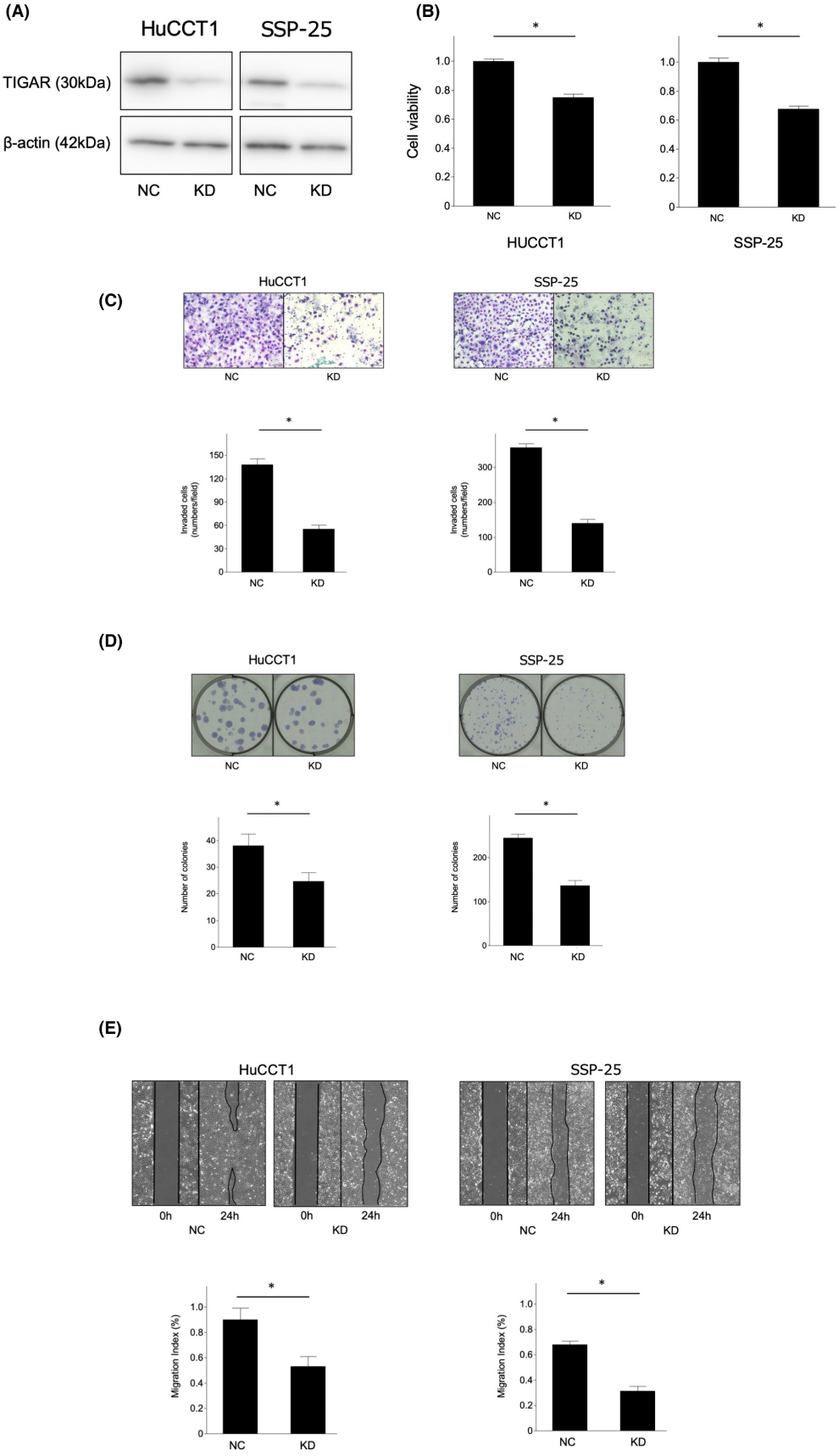

FIGURE 2 TIGAR promotes ICC cell motility. (A) Expression and *TIGAR* KD in cell lines. *TIGAR KD* significantly inhibited cell viability (B), invasion (C), colony formation (D), and migration (E) compared with the negative control (NC). (E) Migration index: 1–[length at 24 h]/[length at 0 h]. *$p < 0.05$. KD, knockdown; NC, negative control; TIGAR, *TP53*-induced glycolysis and apoptosis regulator.

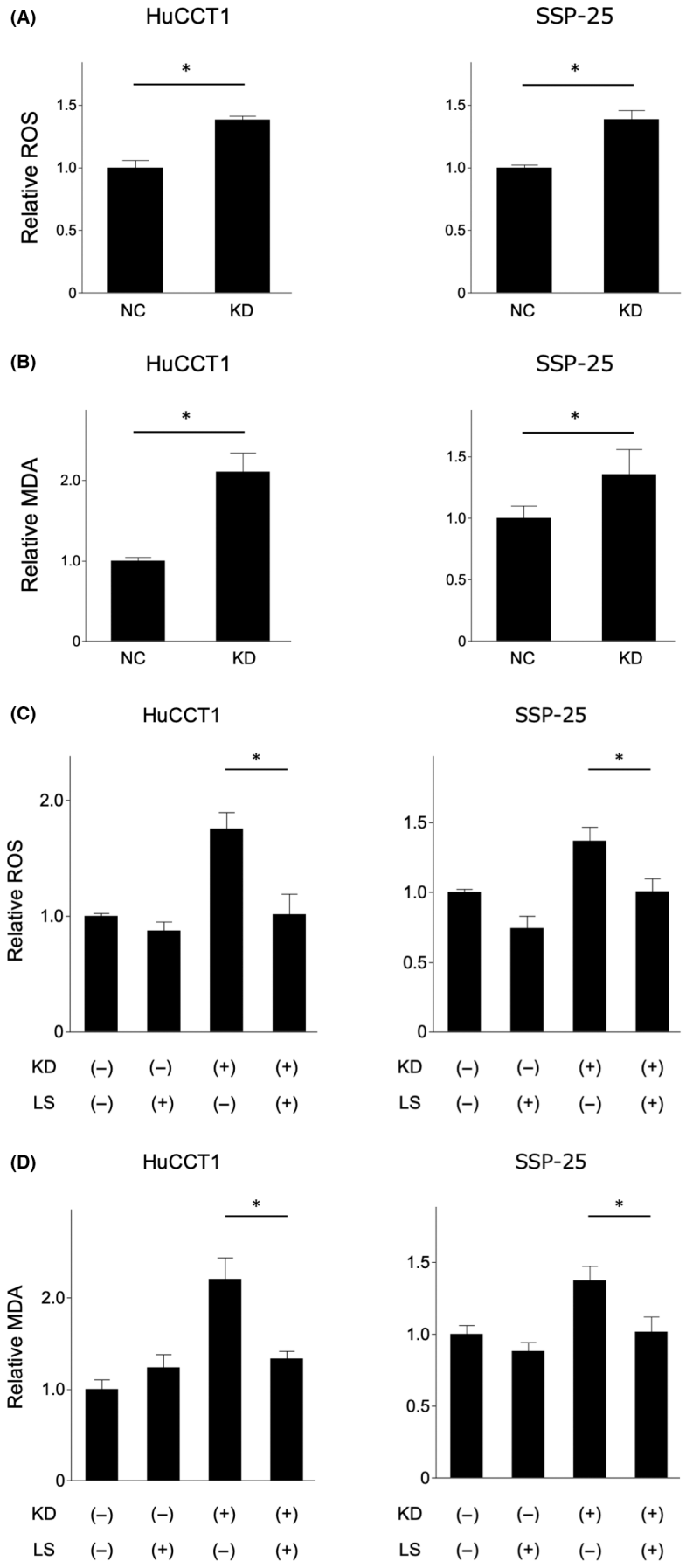

FIGURE 3 (Continued)

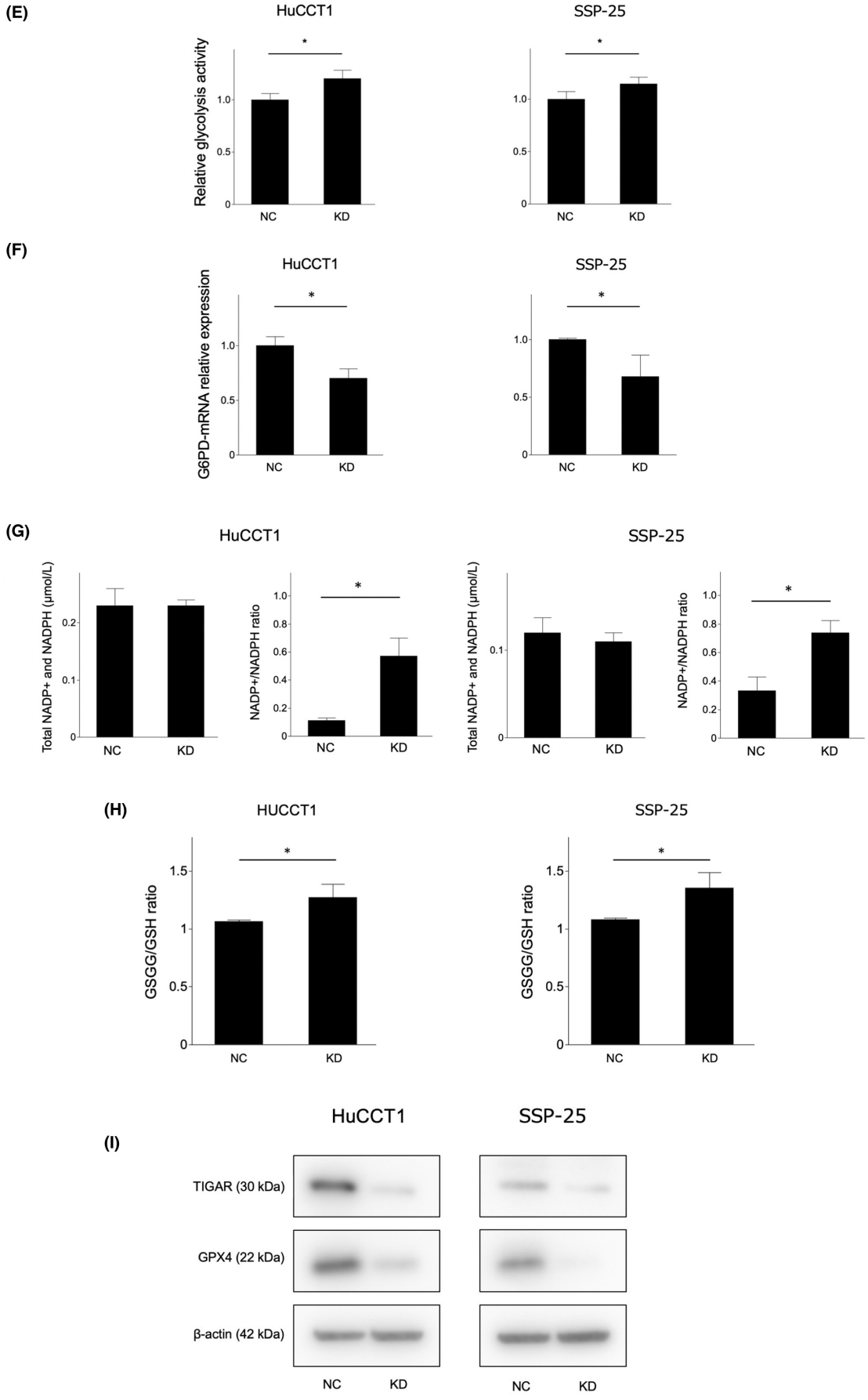

FIGURE 3 (Continued)

FIGURE 3 *TP53*-induced glycolysis and apoptosis regulator (TIGAR) knockdown increases ROS and lipid peroxidation. *TIGAR* KD increased intracellular ROS levels (A) and lipid peroxidation (B). Ferroptosis by TIGAR knockdown was canceled by using 10 μM liproxstatin (C, D). TIGAR KD increased the glycolysis level (E) and decreased G6PD-mRNA expression in RT-PCR (F). *TIGAR* KD increased the NADP+/NADPH ratio (G) and GSGG/GSH ratio (H) and decreased GPX4 protein expression (I). $^*p < 0.05$. G6PD, glucose-6-phosphonate dehydrogenase; GSGG, oxidized glutathione; GSH, reduced glutathione; GPX4, glutathione peroxidase 4; KD, knockdown; LS, liproxstatin; MDA, malondialdehyde; mRNA, messenger ribonucleic acid; NC, negative control; NADP, nicotinamide adenine dinucleotide phosphate; NADPH, nicotinamide adenine dinucleotide phosphate; ROS, reactive oxygen species; TIGAR, *TP53*-induced glycolysis and apoptosis regulator.

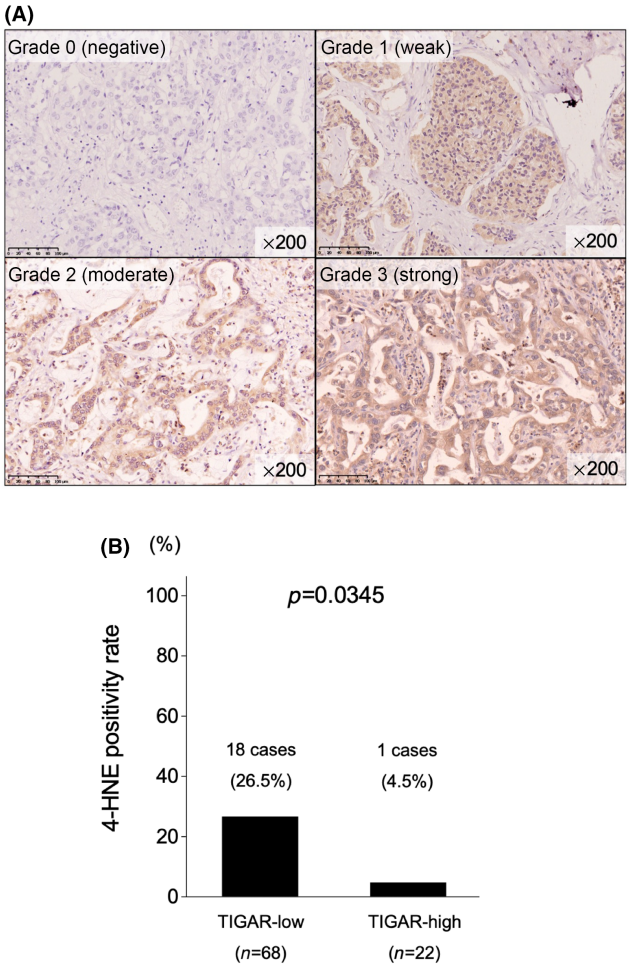

FIGURE 4 4-HNE expression is significantly lower in *TP53*-induced glycolysis and apoptosis regulator (TIGAR)-high group. (A) Immunohistochemical staining of 4-HNE. Grade 0, negative staining; Grade 1, weak staining; Grade 2, moderate staining; Grade 3, strong staining (×200 magnification). (B) 4-HNE positive cases: 18 cases (26.5%) in the TIGAR-low group and one case (4.6%) in the TIGAR-high group ($p = 0.0345$). 4-HNE, 4-hydroxy-2-nonenal; TIGAR, *TP53*-induced glycolysis and apoptosis regulator.

3.10 | Nrf2 is one of the regulators of *TP53*-induced glycolysis and apoptosis regulator expression in intrahepatic cholangiocarcinoma

To investigate whether Nrf2, which has been reported as one of the factors regulating TIGAR expression, is also applicable to ICC, we performed Nrf2 KD using siRNA.[20] TP53 has been reported as upstream of TIGAR, but genetic mutations in TP53 were reported in HuCCT1 and SSP-25 and were not examined. After the confirmation of constant Nrf2 expression in HuCCT1 and SSP-25, we performed Nrf2 KD. As shown in Figure 6A, Nrf2 KD reduced TIGAR expression. In contrast, TIGAR KD did not reduce Nrf2 expression (Figure 6B). These results indicated that Nrf2 is one of the regulators of TIGAR expression in ICC.

4 | DISCUSSION

In the present study, we showed the relationship between TIGAR and poor prognosis in ICC patients after hepatic resection. TIGAR was strongly involved in tumor invasiveness, migration, and proliferation and suppressed ferroptosis by controlling NADPH levels.

TIGAR (c12orf5), as a *TP53*-regulated gene, was originally discovered through induction by ionizing radiation, and its location is mainly in the cytoplasm.[21] There have been many reports on TIGAR and cancer, and *TIGAR* KD was shown to reduce the ability of cells to proliferate.[10,22] In pancreatic cancer in particular, TIGAR has been shown to be dynamically upregulated and downregulated in tumors and to modulate oxidative stress, and knockout of *TIGAR* also reduces the ability of cells to migrate.[8] Although the present study was an in vitro experiment and could not mimic dynamic ROS changes, it was shown that cell motility was reduced in ICC by *TIGAR* KD. The results support that high TIGAR expression is a poor prognostic factor for ICCs, but there were no significant differences in clinicopathological characteristics between the low/high TIGAR expression groups in this study. Few papers have so far shown how TIGAR regulates cell motility, and the relationship between TIGAR and immune cells and cancer-associated fibroblast in actual tumors is one of the issues to be examined in the future. Nrf2 has been reported as one of the regulators of TIGAR in hepatocellular carcinoma, and the results in Figure 5 suggested that Nrf2 was also involved in the regulation of TIGAR in ICC.[20]

Ferroptosis has recently attracted attention as a regulator of oxidative stress in cancer, since Dixon SJ, et al. reported in 2012.[12] ICC accounts for approximately 10% of liver cancer cases and is less common than hepatocellular carcinoma, but the number of patients with ICC has been increasing in recent years; thus, the understanding of its pathogenesis is an urgent issue.[23] Because there are fewer cases compared with hepatocellular carcinoma, research on ferroptosis in ICC is scarce. TIGAR is a critical protein in cellular metabolism, most notably in the regulation of oxidative stress, but there

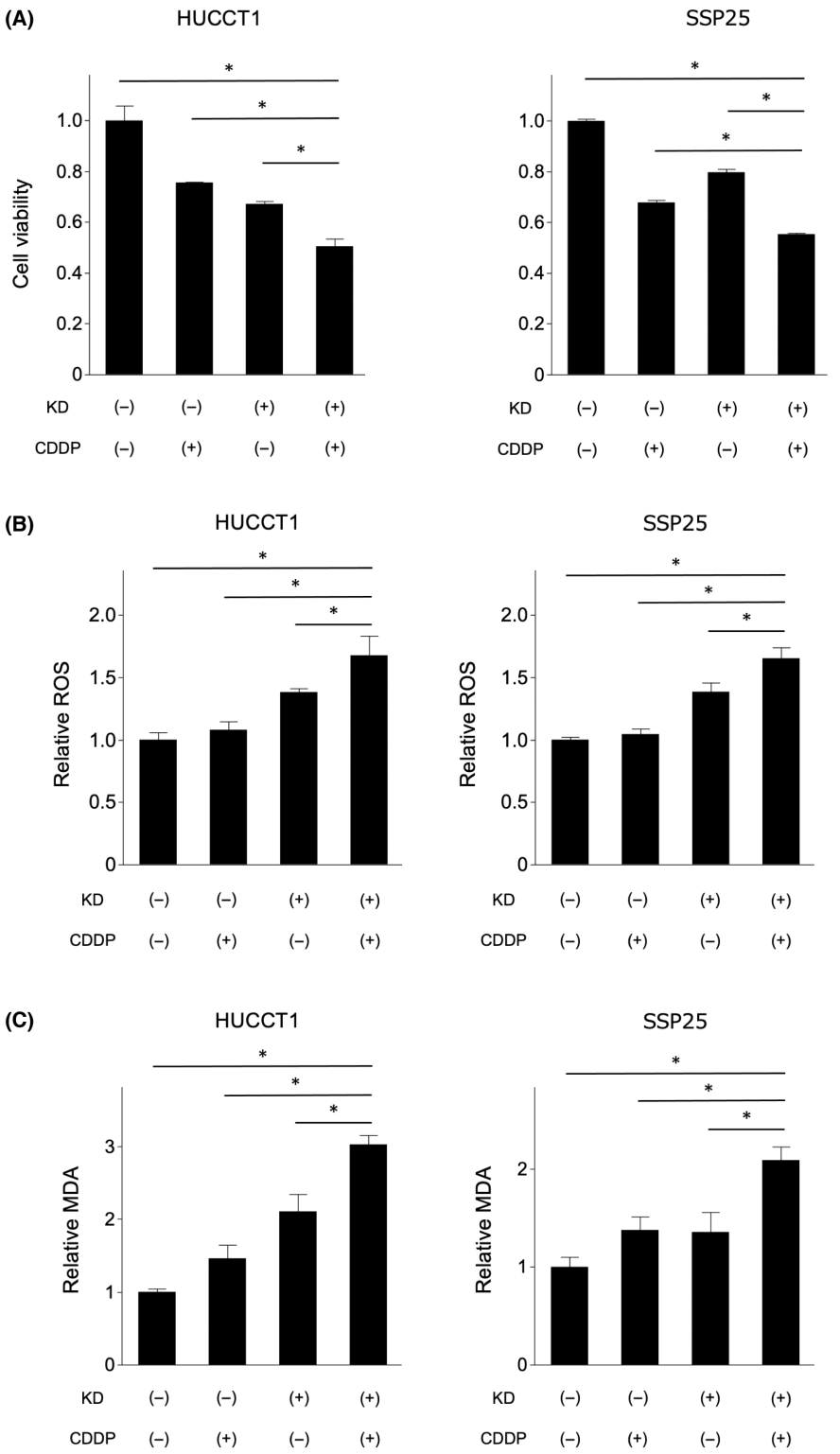

FIGURE 5 Promotion of ferroptosis by *TP53*-induced glycolysis and apoptosis regulator (TIGAR) knockdown in combination with CDDP. The combination of *TIGAR* KD and 10 μM CDDP significantly decreased cell viability (A) and increased the ROS level (B) and lipid peroxidation (C) compared with NC/*TIGAR* KD alone/CDDP alone. $^{*}p < 0.05$. CDDP, cisplatin; KD, knockdown; MDA, malondialdehyde; NC, negative control; ROS, reactive oxygen species; TIGAR, *TP53*-induced glycolysis and apoptosis regulator.

are a small number of reports of its association with ferroptosis.[20] It has been shown that TIGAR activates AMP-activated protein kinase, which is known to inhibit the production of polyunsaturated fatty acid in esophageal cancer, and that TIGAR confers ferroptosis resistance in colon cancer.[10,24] Therefore, we examined whether TIGAR was related to oxidative stress regulatory mechanisms such as ferroptosis in ICC using the GEO dataset and found an association with TIGAR and lipid peroxidation. Our experiments also showed that *TIGAR* KD led to decreased cell viability and increased ROS and MDA levels (i.e., it induced ferroptosis). There are three main requirements in the process of ferroptosis. First, the polyunsaturated fatty acid synthesis pathway is important as a substrate for lipid peroxidation. Second, the accumulation of free intracellular iron and subsequent ROS generation is needed to contribute to lipid peroxidation. Third, the effect of cellular antioxidants including system Xc^- (xCT) and GPX4 needs to be reduced: these mechanisms

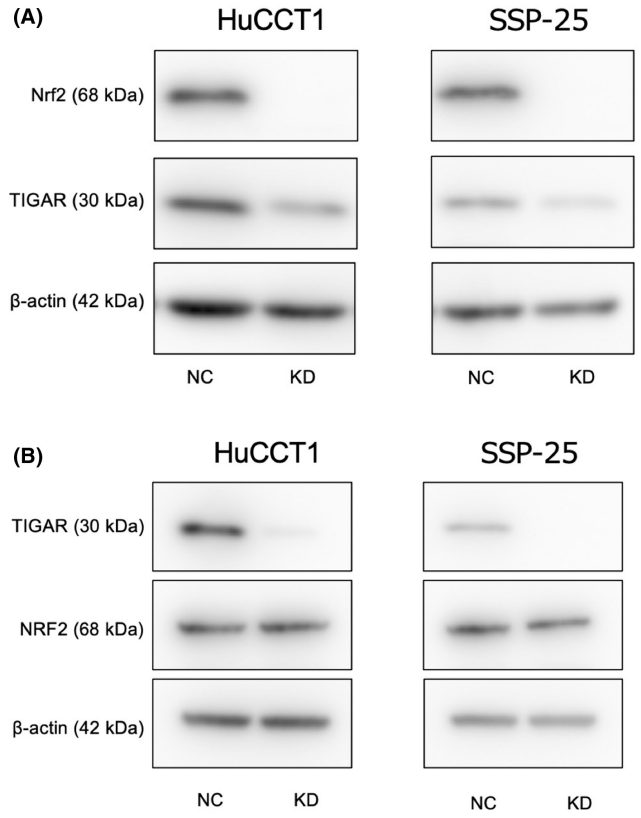

FIGURE 6 Nrf2 regulates *TP53*-induced glycolysis and apoptosis regulator (TIGAR) expression in ICC. (A) Nrf2 KD reduced TIGAR expression in WB analysis. (B) TIGAR KD did not reduce Nrf2 expression in WB analysis. ICC, intrahepatic cholangiocarcinoma; KD, knockdown; Nrf2, nuclear factor erythroid 2-related factor 2; TIGAR, *TP53*-induced glycolysis and apoptosis regulator. WB, western blot.

work together to induce ferroptosis.[25] In this study, we focused on the ability of TIGAR to produce NADPH because TIGAR has the function of promoting the pentose phosphate circuit and producing NADPH, an important reducing agent. We showed that *TIGAR* KD increased the NADP/NADPH ratio (i.e., decreased NADPH-producing capacity), followed by an increased GSGG/GSH ratio and decreased GPX4 protein expression. Thus, we demonstrated that TIGAR has a ferroptosis inhibitory effect by decreasing the production of GPX4 downstream of xCT. In addition to ferroptosis, *TIGAR* KD also induced apoptosis: TIGAR can induce two cell death mechanisms simultaneously, making TIGAR a potentially important therapeutic target in ICC.

CDDP exerts anticancer activity via multiple mechanisms, but its most acceptable mechanism involves the generation of DNA lesions by interacting with purine bases on DNA, and it has been used for systemic therapy of ICC.[26] In addition, CDDP is known not only for its role in generating ROS but also for inducing ferroptosis by inhibiting GPX4 production, similar to TIGAR in this study.[27,28] In fact, our study found an increase in ROS and MDA even with CDDP alone, suggesting that the strong reduction in inhibition by both *TIGAR* KD and CDDP strongly induced ferroptosis.

A limitation of this study was its single-center retrospective design with a relatively small study cohort to examine prognostic factors influencing DFS and OS. Further large-scale studies are warranted in the future.

In conclusion, we demonstrated that TIGAR was associated with poor outcomes in ICC patients after curative hepatic resection and with resistance to ferroptosis.

AUTHOR CONTRIBUTIONS

Katsuya Toshida: Conceptualization; data curation; formal analysis; investigation; methodology; project administration; writing – original draft. **Shinji Itoh:** Conceptualization; data curation; formal analysis; funding acquisition; investigation; methodology; project administration; supervision; visualization; writing – original draft; writing – review and editing. **Norifumi Iseda:** Data curation; formal analysis. **Takuma Izumi:** Data curation; formal analysis. **Shohei Yoshiya:** Data curation; formal analysis. **Takeo Toshima:** Conceptualization; data curation; formal analysis. **Mizuki Ninomiya:** Data curation; formal analysis; investigation. **Takeshi Iwasaki:** Investigation. **Yoshinao Oda:** Supervision. **Tomoharu Yoshizumi:** Supervision.

ACKNOWLEDGMENTS

We thank Ms. Saori Tsurumaru, Ms. Asuka Nakamura, Ms. Yuko Kubota, and Ms. Miki Nakashima for technical support. We thank H. Nikki March, PhD, from Edanz (https://jp.edanz.com/ac) for editing a draft of this manuscript.

FUNDING INFORMATION

This study was supported by JSPS KAKENHI (grant numbers JP-19K09198 and JP-23K08133), the Takeda Science Foundation, and the Kobayashi Foundation for Cancer Research. The funding sources had no role in the collection, analysis, or interpretation of the data or in the decision to submit the article for publication.

CONFLICT OF INTEREST STATEMENT

Y.O. is an Editorial Board Member of *Cancer Science*. The other authors have no conflict of interest.

ETHICS STATEMENTS

Approval of research protocol by an Institutional Reviewer Board: This study was approved by the Clinical Research Ethics Committee of Kyushu University (approval code: 2021-467).

Informed Consent: All participants provided written informed consent.

Registry and Registration No. of the study/trial: N/A.

Animal Studies: N/A.

ORCID

Shinji Itoh https://orcid.org/0000-0003-0382-2520
Takeo Toshima https://orcid.org/0000-0003-4019-8288
Yoshinao Oda https://orcid.org/0000-0001-9636-1182

REFERENCES

1. Banales JM, Marin JJG, Lamarca A, et al. Cholangiocarcinoma 2020: the next horizon in mechanisms and management. *Nat Rev Gastroenterol Hepatol*. 2020;17:557-588.

2. Khan SA, Davidson BR, Goldin RD, et al. Guidelines for the diagnosis and treatment of cholangiocarcinoma: an update. *Gut*. 2012;61:1657-1669.
3. Yugawa K, Itoh S, Yoshizumi T, et al. Lymphocyte-C-reactive protein ratio as a prognostic marker associated with the tumor immune microenvironment in intrahepatic cholangiocarcinoma. *Int J Clin Oncol*. 2021;26:1901-1910.
4. Valle J, Wasan H, Palmer DH, et al. Cisplatin plus gemcitabine versus gemcitabine for biliary tract cancer. *N Engl J Med*. 2010;362:1273-1281.
5. Toshida K, Itoh S, Yugawa K, et al. Prognostic significance for recurrence of fibroblast growth factor receptor 2 in intrahepatic cholangiocarcinoma patients undergoing curative hepatic resection. *Hepatol Res*. 2023;53:432-439.
6. Yugawa K, Yoshizumi T, Mano Y, et al. Cancer-associated fibroblasts promote hepatocellular carcinoma progression through downregulation of exosomal miR-150-3p. *Eur J Surg Oncol*. 2021;47:384-393.
7. Bensaad K, Tsuruta A, Selak MA, et al. TIGAR, a p53-inducible regulator of glycolysis and apoptosis. *Cell*. 2006;126:107-120.
8. Cheung EC, DeNicola GM, Nixon C, et al. Dynamic ROS control by TIGAR regulates the initiation and progression of pancreatic cancer. *Cancer Cell*. 2020;37:168-182.e164.
9. Won KY, Lim SJ, Kim GY, et al. Regulatory role of p53 in cancer metabolism via SCO2 and TIGAR in human breast cancer. *Hum Pathol*. 2012;43:221-228.
10. Liu MY, Li HM, Wang XY, et al. TIGAR drives colorectal cancer ferroptosis resistance through ROS/AMPK/SCD1 pathway. *Free Radic Biol Med*. 2022;182:219-231.
11. Dixon SJ, Lemberg KM, Lamprecht MR, et al. Ferroptosis: an iron-dependent form of nonapoptotic cell death. *Cell*. 2012;149:1060-1072.
12. Lei G, Zhuang L, Gan B. Targeting ferroptosis as a vulnerability in cancer. *Nat Rev Cancer*. 2022;22:381-396.
13. Itoh S, Shirabe K, Taketomi A, et al. Zero mortality in more than 300 hepatic resections: validity of preoperative volumetric analysis. *Surg Today*. 2012;42:435-440.
14. Itoh S, Yoshizumi T, Yugawa K, et al. Impact of immune response on outcomes in hepatocellular carcinoma: association with vascular formation. *Hepatology*. 2020;72:1987-1999.
15. Song Y, Wang PY, Zheng Y, Liu C, Wang XM. Expression of TIGAR and its correlation with clinicopathology, prognosis, and 18F-FDG PET/CT parameters in patients with resectable pancreatic ductal adenocarcinoma. *Nucl Med Commun*. 2021;42:528-534.
16. Podszun MC, Chung JY, Ylaya K, Kleiner DE, Hewitt SM, Rotman Y. 4-HNE immunohistochemistry and image analysis for detection of lipid peroxidation in human liver samples using vitamin E treatment in NAFLD as a proof of concept. *J Histochem Cytochem*. 2020;68:635-643.
17. Itoh S, Taketomi A, Harimoto N, et al. Antineoplastic effects of gamma linolenic acid on hepatocellular carcinoma cell lines. *J Clin Biochem Nutr*. 2010;47:81-90.
18. Iseda N, Itoh S, Toshida K, et al. Ferroptosis is induced by lenvatinib through fibroblast growth factor receptor-4 inhibition in hepatocellular carcinoma. *Cancer Sci*. 2022;113:2272-2287.
19. Lin W, Tsai WL, Shao RX, et al. Hepatitis C virus regulates transforming growth factor beta1 production through the generation of reactive oxygen species in a nuclear factor kappaB-dependent manner. *Gastroenterology*. 2010;138:2509-2518.e1.
20. Simon-Molas H, Sánchez-de-Diego C, Navarro-Sabaté À, et al. The expression of TP53-induced glycolysis and apoptosis regulator (TIGAR) can Be controlled by the antioxidant orchestrator NRF2 in human carcinoma cells. *Int J Mol Sci*. 2022;23:1905.
21. Bensaad K, Cheung EC, Vousden KH. Modulation of intracellular ROS levels by TIGAR controls autophagy. *EMBO J*. 2009;28:3015-3026.
22. Zhao D, Qian L, Zhuang D, et al. Inhibition of ribosomal RNA processing 15 homolog (RRP15), which is overexpressed in hepatocellular carcinoma, suppresses tumour growth via induction of senescence and apoptosis. *Cancer Lett*. 2021;519:315-327.
23. Florio AA, Ferlay J, Znaor A, et al. Global trends in intrahepatic and extrahepatic cholangiocarcinoma incidence from 1993 to 2012. *Cancer*. 2020;126:2666-2678.
24. Chu J, Niu X, Chang J, et al. Metabolic remodeling by TIGAR overexpression is a therapeutic target in esophageal squamous-cell carcinoma. *Theranostics*. 2020;10:3488-3502.
25. Bekric D, Ocker M, Mayr C, et al. Ferroptosis in hepatocellular carcinoma: mechanisms, drug targets and approaches to clinical translation. *Cancers (Basel)*. 2022;14:1826.
26. Ghosh S. Cisplatin: the first metal based anticancer drug. *Bioorg Chem*. 2019;88:102925.
27. Mirzaei S, Hushmandi K, Zabolian A, et al. Elucidating role of reactive oxygen species (ROS) in cisplatin chemotherapy: a focus on molecular pathways and possible therapeutic strategies. *Molecules*. 2021;26:2382.
28. Guo J, Xu B, Han Q, et al. Ferroptosis: a novel anti-tumor action for cisplatin. *Cancer Res Treat*. 2018;50:445-460.

SUPPORTING INFORMATION

Additional supporting information can be found online in the Supporting Information section at the end of this article.

How to cite this article: Toshida K, Itoh S, Iseda N, et al. Impact of *TP53*-induced glycolysis and apoptosis regulator on malignant activity and resistance to ferroptosis in intrahepatic cholangiocarcinoma. *Cancer Sci*. 2024;115:170-183. doi:10.1111/cas.15981